AD-A160 497 EFFECTS OF BLADE-TO-BLADE DISSIMILARITIES ON ROTOR-BODY 1/1
LEAD-LAG DYNAMICS(U) ARMY AVIATION RESEARCH AND
TECHNOLOGY ACTIVITY MOFFETT FIELD C.. M J MCNULTY 1985
UNCLASSIFIED F/G 1/3 NL

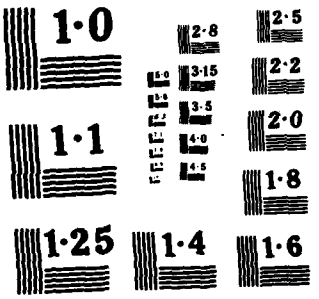
1·0
1·1
1·25
2·8
3·15
3·5
4·0
4·5
2·5
2·2
2·0
1·8
1·4
1·6

(1)

ELEVENTH EUROPEAN ROTORCRAFT FORUM

Paper No. 64

EFFECTS OF BLADE-TO-BLADE DISSIMILARITIES ON ROTOR-BODY LEAD-LAG DYNAMICS

Michael J. McNulty

Aeroflightdynamics Directorate
U.S. Army Aviation Research and Technology Activity-AVSCOM
Ames Research Center
Moffett Field, CA

September 10-13, 1985

London, England

THE CITY UNIVERSITY, LONDON, EC1V OHB, ENGLAND

EFFECTS OF BLADE-TO-BLADE DISSIMILARITIES ON ROTOR-BODY LEAD-LAG DYNAMICS

Michael J. McNulty
Aeroflightdynamics Directorate
U.S. Army Aviation Research and Technology Activity
Ames Research Center
Moffett Field, California 94035, U.S.A.

ABSTRACT

Small blade-to-blade property differences are investigated to determine their effects on the behavior of a simple rotor-body system. An analytical approach is used which emphasizes the significance of these effects from the experimental point of view. It is found that the primary effect of blade-to-blade dissimilarities is the appearance of additional peaks in the frequency spectrum which are separated from the conventional response modes by multiples of the rotor speed. These additional responses are potential experimental problems because when they occur near a mode of interest they act as contaminant frequencies which can make damping measurements difficult. The effects of increased rotor-body coupling and a rotor shaft degree of freedom act to improve the situation by altering the frequency separation of the modes.

1. *NOMENCLATURE*

c_i	lead-lag damper constant of blade i, N-m-sec
c_s	damper constant of the rotor shaft degree of freedom, N-m-sec
c_x	damper constant of the x body degree of freedom, N-sec/m
c_y	damper constant of the y body degree of freedom, N-sec/m
e_i	distance from the hub center to the hinge of blade i, m
I_i^*	lead-lag inertia of blade i about its own mass center, kg-m^2
I_s	inertia of the rotor shaft about the hub center, kg-m^2
k_i	lead-lag spring constant of blade i, N-m
k_s	spring constant of the rotor shaft degree of freedom, N-m
k_x	spring constant of the x body degree of freedom, N/m
k_y	spring constant of the y body degree of freedom, N/m
l_i^*	distance from hinge to mass center of blade i, m
m_i	mass of blade i, kg

m_x	effective mass of the x body degree of freedom, kg
m_y	effective mass of the y body degree of freedom, kg
N	number of blades
s	rotor shaft degree of freedom
t	time, sec
x	body translational degree of freedom
y	body translational degree of freedom, normal to x
ψ_i	$2\pi(i-1)/N$
ζ_i	blade i lead-lag angle
ζ_o	multiblade collective coordinate
ζ_c	multiblade cosine coordinate
ζ_s	multiblade sine coordinate
Ω	rotor speed, constant, 1/sec
$(\dot{\ })$	derivative with respect to t

2. *INTRODUCTION*

In the course of a recent experimental study of the lead-lag stability of a model rotor conducted by the Aeroflightdynamics Directorate, difficulties in measuring damping were encountered for a system whose relevant modes were well separated, *i.e.* by approximately 2/rev. This measurement problem was similar to that caused by the contamination of data by another closely spaced mode. This experimental problem was eliminated then by carefully matching the blade-to-blade properties. Further analysis of this problem led to an investigation of the dynamics of rotor-body systems in which the blade properties differ slightly from one blade to the next. Barring mechanical failure or damage, helicopter blades are sufficiently matched that the assumption of identical blades would not significantly affect any analysis of the basic dynamic characteristics of the system; however, blade-to-blade dissimilarities are potentially a factor in several interesting and relevant problems. In particular, helicopter 1/rev vibration levels and the quality of experimental data in model and flight test programs could be affected by small differences in properties between blades. Only the experimental data quality issue is addressed in the present work.

Coleman and Feingold's work on rotor-body lead-lag dynamics [1] showed that if either the body is isotropic or the rotor has polar symmetry (*i.e.*, the rotor has three or more blades, all with identical properties) a transformation to multiblade coordinates [2] exists which will eliminate the periodic coefficients which come from writing the equations of motion in terms of both rotating and nonrotating coordinate systems. They also showed that, for the isotropic rotor case, any blade motions which could couple with a rotor shaft rotational degree of freedom do not couple with the body translational motion and can therefore be considered separately. However, for nonisotropic bodies, if the rotor blades

are not identical the periodic coefficients cannot be eliminated and in general the rotor, body, and drive system dynamics are coupled.

Floquet's theorem describes the solutions of linear differential equations with periodic coefficients, and the use of Floquet theory in rotorcraft dynamics is well established. References 3 and 4, for example, deal with periodic coefficients due to forward flight, and reference 5 considers a rigid two-bladed rotor with shaft bending flexibility as well as body degrees of freedom. These works all use the Floquet transition matrix to obtain the system eigenvalues and find stability boundaries. Hammond [6] considered a four-bladed articulated rotor on a nonisotropic body which had periodic coefficients as a result of one blade damper being inoperative. While some time history results are presented, the emphasis in reference 6 is also on eigenvalues. The effect of a rotor shaft degree of freedom was not investigated in reference 6.

The occurence of individual modes which contain responses at multiple frequencies separated by multiples of the rotor speed is a prediction of Floquet's theorem. This phenomenon of "multivalued frequencies" is rigorously understood as a response composed of a periodic mode shape with the same period as the coefficients of the governing differential equations, which is then multiplied by an exponential damping term and a sinusiodal term with a "natural frequency" which will always be less than 1/rev. The analyst is free to add any multiple of the rotor speed to the "natural frequency" so long as the frequency content of the periodic mode shape is adjusted to leave the product of the two unchanged. In practice, enough multiples of the rotor speed are usually added so that what are then called the natural frequencies of the system are obviously associated with the frequencies of an appropriate constant coefficient system. This procedure is mathematically correct and physically appealing, but seems to have led to a certain amount of confusion on some parts about this seemingly ambiguous frequency. This is probably due to the fact that most published Floquet results concentrate on eigenvalues and pay little attention to the periodic eigenvectors or time or frequency domain results.

The objective of this investigation is to examine the effects of blade-to-blade dissimilarities on the dynamics of a simple rotor-body system from the standpoint of how the behavior of such a system would manifest itself physically. The emphasis here is on gaining physical insight into the effects of the dissimilarities on the response of the system and noting when these effects could be problems in an experimental setting, rather than on determining how the dissimilarities affect the actual analytical eigenvalues. Two different body configurations are examined, and the effect of including a rotor shaft degree of freedom is considered. The approach taken is to numerically integrate the equations of motion, and then use time and frequency domain data analysis techniques on the resulting time histories. While this approach is inferior to a Floquet eigenanalysis for determining system frequency and damping values, both in terms of accuracy and efficiency, it has the advantage of giving more insight into possible experimental problems. Looking at this simple Floquet system in this manner should also help to clarify the meaning of the "multivalued frequency" result of Floquet theory.

2. *ANALYSIS*

The model considered herein consists of a body with two translational degrees of freedom, x and y, each of which has an effective mass, spring, and damper. The rotor shaft, with inertia I_s, rotates at an angular speed of $(\Omega + \dot{s})$ where Ω is a constant and s is a rotor shaft angular perturbation degree of freedom. This shaft rotational degree of freedom also has a spring and damper associated with it, attached to the constant Ω "ground". The rotor itself consists of N rigid blades with spring and damper restraints, each of which is free to move in lead-lag about an offset hinge. The mass properties, hinge offset, and spring and damper constants of any blade are not necessarily the same as those of any other blade. A schematic of this system is shown in figure 1.

The differential equations of motion for the system above were derived and programmed in a form suitable for solution in the time domain using a numerical integration routine, and they are included in the appendix. The program allowed the x, y, and s degrees of freedom each to be included, locked out entirely, or constrained to move sinusoidally at a specified amplitude and frequency, as desired. The integration itself was carried out in two phases; an excitation phase and a transient phase. During the first phase some combination of applied forces, specified body motions, and initial conditions was used to excite the system, then, at a designated time, the excitation was terminated and thereafter the transient response of the system was calculated. Each computed time history was 10.24 sec long with data at 0.005 sec intervals.

The solution results were obtained in the form of time histories of the individual blade and body motions. In order to remove the periodic coefficient effects associated solely with the use of both rotating and nonrotating coordinate systems and to allow comparison with past rotor-body dynamics work, the time history results were post-processed to transform them to the multiblade coordinate system [2]. For three blades, and allowing for the shaft degree of freedom, s, this transformation is defined as:

$$\zeta_o = \frac{1}{3}\sum_{i=1}^{3}\zeta_i \tag{1}$$

$$\zeta_c = \frac{2}{3}\sum_{i=1}^{3} cos(\Omega t + \psi_i + s)\zeta_i \tag{2}$$

$$\zeta_s = \frac{2}{3}\sum_{i=1}^{3} sin(\Omega t + \psi_i + s)\zeta_i \tag{3}$$

Equations (2) and (3) reduce to the usual definition of the multiblade transform for small s perturbations.

The blade properties used in this investigation were chosen to represent blades that have been used for some experiments conducted by the Aeroflightdynamics Directorate.

The body properties were chosen to represent the rotor test stand which is used in conjunction with these blades. This stand has two possible configurations; one with a relatively soft flexural element restraining the body x degree of freedom, and a second in which a clamp is used to further restrain the body x motions, giving a much stiffer system. These two configurations are referred to as the soft and stiff bodies, respectively. Both of these configurations are very stiff in the y direction. The rotor shaft properties used were based on estimates of the drive system properties associated with this stand. The model properties used for this investigation are summarized in table 1.

The system frequency and damping values were determined from the computed time histories via spectral analysis and the moving-block technique [7]. While this approach is inferior to a Floquet eigenanalysis with regard to computation time, it duplicates the experimental data analysis and it has the advantage of giving the same kind of insight into the behavior of the physical system that an experiment would. It is believed that this is approach is particularly helpful in understanding the periodic mode shapes, or "multivalued frequencies" which occur for periodic coefficient systems.

A variable-order, variable-stepsize, numerical integration method was used for the present work with the belief that it would be a more sophisticated method than this problem actually called for. As a checkout of the program, the case of the nonisotropic body with one blade damper inoperative from reference 6 was run. The results of the spectral analysis and moving-block technique agreed very well with the Floquet eigenanalysis results shown in figure 5 of reference 6.

3. *RESULTS*

Matched Blades

To demonstrate the baseline system behavior, system frequencies are shown as a function of rotor speed in figure 2 for the soft body configuration with three identical blades. The data points shown were obtained by applying a sinusoidal force to the x body degree of freedom at approximately the progressing or regressing mode frequency, or by using a small x displacement as an initial condition, as required. The fixed system blade frequencies for the isolated rotor case are shown for comparison as the dashed lines. Because of coupling with the body, the lead-lag progressing mode frequency is about 2 Hz above the isolated rotor result, and the the lead-lag regressing and progressing modes are not 2/rev apart, as they must be for the isolated rotor case. The rotor shaft degree of freedom was not included because it does not affect the results. It is worth emphasizing that although the system has five degrees of freedom the nonrotating multiblade coordinates, ζ_c and ζ_s, will only participate in four modes. The only multiblade coordinate in which the fifth mode will appear is the collective coordinate, ζ_0, and the modes which appear in ζ_c and ζ_s will not appear there. The frequencies of the stiff body with three identical blades are shown in figure 3. Even though the body frequencies were fairly high for this configuration, above 45 Hz, the progressing mode still diverges from the isolated blade results above about 500 rpm. Although no results are presented here, the moving-block

analysis can be expected to give very good results for both configurations, because there are no closely spaced modes which could interfere with each other.

Figures 4 and 5 are included mainly for comparison with the mismatched blade results which follow. Figure 4(a) shows the frequency domain response of the ζ_c coordinate to a small initial displacement of the body x degree of freedom as a function of the rotor speed, for the soft body configuration. This type of excitation was chosen because it can be applied consistently at any rpm and so any differences in the response from one rotor speed to another are due solely to the changing properties of the system, not changing excitation. The disadvantages of this type of excitation is that it does not excite the body y mode very well until the rotor speed is high enough for gyroscopic coupling to become important, and it tends to emphasize the modes whose natural frequencies are closer to that of the body x mode. In particular, the lead-lag regressing mode is not as well excited as the progressing mode, especially at rotor speeds where the regressing mode frequency is very low. Figure 4(b) identifies the peaks shown in figure 4(a) at 1000 rpm. Figures 5(a) and 5(b) give the same information for the stiff body configuration. For both cases the body y mode is more apparent at the higher rotor speeds because the gyroscopic coupling between the two body degrees of freedom is small at the lower rotor speeds. The ragged appearance of the progressing and regressing ridges in these plots and the plots to follow has no physical significance; it is purely a result of the way that the plotting routine interpolates between data points when constructing the surface. The rough appearance of the y mode peak at the lower rotor speeds in figure 5(b) is due to computational noise. No response plots are given for the collective coordinate because, for this case, its response is zero.

Mismatched Blades, No Shaft Degree of Freedom

To examine the effects of blade-to-blade dissimilarities, the inertia of blade one about its own mass center, I_1^*, was increased enough to lower the nonrotating, isolated blade frequency of this blade by 4%. Because 1/rev body motions caused by unbalance were not desired, the blade mass and mass center location were unchanged. Responses to regressing excitation, progressing excitation, and an x body initial condition were then computed for both body configurations without the rotor shaft degree of freedom.

The frequency results for the multiblade cosine coordinate obtained from these computations are shown in figure 6 for the soft body, corresponding to the matched blade results of figure 2. Any peak that could be found in response to regressing or progressing excitation, or to a body x initial condition was included. If a point is missing from where the trends would lead one to expect to find it, it does not mean that that response does not exist, just that it could not be observed because its amplitude was too low or perhaps because it was obscured by a larger nearby peak. The results for the regressing and progressing lead-lag modes and for the body x and y modes are only slightly altered from the matched blade results. Some small changes are expected since the system's overall physical properties were slightly altered by increasing the one blade's inertia. The obvious change from the matched blade case is the appearance of many additional peaks in the spectrum corresponding to the frequencies of the expected modes $\pm$ M/rev.

In addition, responses are found that are not associated with any mode which involved the cosine coordinate for the matched blade case. In particular the response slightly below the regressing lead-lag mode and the response 2/rev above this (about 2 Hz below the progressing lead-lag mode) are associated with the rotor collective lead-lag mode, shifted ± 1/rev. (At 200 and 300 rpm, response at the collective frequency plus 3/rev was also measurable.) This 1/rev shift is associated with changing from the rotating ζ_o coordinate to the nonrotating ζ_c coordinate. These responses are slightly different from the matched blade uncoupled rotor frequencies because the inertia added to the one blade changes the coupled collective mode frequency slightly.

Both these types of side peaks are the physical manifestations of the periodic mode shapes associated with this periodic coefficient system. In general, it was found that in a single coordinate the individual elements of the periodic mode shapes were always separated by multiples of 2/rev, while comparing results between rotating and nonrotating coordinates introduces and extra 1/rev shift, giving odd/rev separations. These periodic mode shapes and the coupling which occurs through them between the multiblade ζ_o coordinate and the non-rotating multiblade coordinates is better illustrated by figures 7 and 8. Figure 7(a) shows the frequency domain response in the ζ_c coordinate to an x body initial condition as a function of rotor speed, and figure 7(b) identifies the resulting peaks for the 1000-rpm case. A comparison with figure 4 shows that the mismatch has only slighty changed the system's fundamental dynamic properties, as evidenced by the location and shape of the peaks corresponding to the matched blade results, but the periodic mode shapes give rise to a much more complex spectrum. The most significant result of this is in the vicinity of the lead-lag regressing mode peak, where both a collective mode minus 1/rev and a progressing mode minus 2/rev peak have come about because of the mismatch. The existence of these extraneous peaks very near a mode of interest can be expected to cause problems with widely used experimental damping measurement techinques which are based on single-degree-of-freedom assumptions [7]. The progressing mode can be expected to be less seriously affected by the collective plus 1/rev peak near it because the frequency separation between the two is greater, due to the coupling between the progressing mode and the body which shifts the progressing mode frequency away from the isolated rotor result and hence away from the collective mode plus 1/rev peak.

The response seen in the ζ_o coordinate for these same cases is shown in figure 8. Without the mismatch this coordinate does not respond at all to fixed system excitation, but it can be seen that the blade-to-blade mismatch not only allows the collective mode to respond to fixed system excitation, but also causes the fixed system modes to appear in the collective coordinate shifted by ± 1/rev.

The results for these same conditions, but with the stiff body, are now considered. The frequencies at which responses were found in the ζ_c coordinate for the stiff body configuration are shown in figure 9. Because the stand frequencies are relatively high, the rotor modes now fall closer to the isolated blade results, especially at the lower rotor speeds. This means that the progressing and regressing lead-lag modes are closer to 2/rev apart from each other, and closer to 1/rev apart from the collective mode than they were for the soft body case. This means that the periodic mode shape responses caused by the

mismatch are now located closer to the modes of interest and any data analysis problems will be exacerbated.

Neither the soft nor the stiff body configurations was ever found to produce a measureable response at the regressing mode frequency plus 2/rev. It is believed that it is present but is being masked by the collective mode plus 1/rev response. It should also be noted that the collective mode plus 1/rev response could not be found at 800 rpm and that this is likely related to the regressing mode frequency becoming zero near that rotor speed. Figures 10 and 11 show the frequency domain response to an x initial condition for the multiblade cosine and collective coordinates respectively for the stiff body configuration, as in figures 7 and 8 for the soft body.

Effect of the Shaft Degree of Freedom

The effect of the rotor shaft degree of freedom combined with the 4% frequency mismatch was investigated for both body configurations using the shaft properties shown in table 1. Figures 12 and 13 show the resulting frequencies which could be observed in the ζ_c coordinate for the soft and stiff bodies, respectively (corresponding to figures 6 and 9 without the shaft). The most significant result of the addition of the shaft degree of freedom is that the collective mode $\pm$ 1/rev responses can no longer be observed in the cosine coordinate. The regressing lead-lag mode still has the progessing mode minus 2/rev peak nearby, and the progressing mode still has the regressing mode plus 2/rev nearby, but for both body configurations the frequency separation is now great enough that, at least at most rotor speeds, the two mode damping measurement problem should be managable [7]. Note that for the cases without the shaft the peak which paralleled the progressing mode was identified as the collective mode plus 1/rev, while for the cases with the shaft degree of freedom this peak has been identified as the regressing mode plus 2/rev. This classification was based on careful frequency measurements and this result is evidence that the regressing mode plus 2/rev response does occur for the no-shaft cases, but that it is obscured by the collective plus 1/rev mode, as suggested above.

The multiblade cosine coordinate response to an x body initial condition at 1000 rpm is shown in figure 14(a) for the soft body and in figure 14(b) for the stiff body. These results are directly comparable to figures 7(b) and 10(b), respectively, the only differences being due to the inclusion of the shaft in the present case. For both body configurations with the shaft free, the regressing mode's peak shape gives no reason to expect any measurement problems, and the combined effects of the shaft and the mismatch have shifted the regressing mode frequency slightly (by about 0.2 Hz). Again, without mismatch the rotor shaft freedom does not affect either the progressing or regressing modes.

The response in the multiblade collective coordinate for the soft and stiff bodies respectively are shown in Figures 15 and 16. Whereas for the cases without shaft freedom a single multiblade collective mode appears very close to the isolated blade frequency, the addition of the shaft degree of freedom gives rise instead to two modes, labeled s_1 and s_2, involving rotor shaft and blade collective coordinate motion at frequncies of 5.1 and 34.1 Hz at 0 rpm, increasing to 5.5 and 46.2 Hz at 1000 rpm. The fact that these modes are now well removed from the isolated blade frequency explains why the cosine coordinate peaks

are not contaminated: neither s_1 nor $s_2 \pm 1$/rev falls near the progressing or regressing mode frequencies as was the case without shaft freedom (and particularly so with the stiff body). Even if the s_1 or s_2 modes did appear in the cosine coordinate, they would not be in a position to necessarily cause difficulties. This conclusion should hold over a wide range a shaft spring and inertia values, but if I_s is low and k_s is very high, then s_1 will approach the uncoupled blade frequency; and if I_s very high while k_s is low, then s_2 will approach the uncoupled blade frequency. In either case the potential then exists for behavior similar to the no-shaft case.

Effect of Varying Mismatch

Figure 17 is included to briefly show the effect of varying mismatch. For the soft body configuration at 1000 rpm without the shaft degree of freedom, the cosine coordinate response to progressing mode excitation is shown as the frequency mismatch (caused by increasing I_1^*) varies from 0 to 5%. It is seen that the mismatch only slightly changes the frequencies of the expected peaks, but that the amplitude of the M/rev shifted side peaks increases with increasing mismatch. Because the amplitude is plotted on a logarithmic scale in figure 17, it appears that these side peaks increase rapidly for small amounts of mismatch and then level off. To better show the true amplitude of a side peak as mismatch is increased figure 18 is included to show the amplitude of the progressing plus 2/rev peak as a function of mismatch with a linear amplitude scale. This shows that the amplitude varies more uniformly with mismatch than figure 17 implied. The figure 18 results are significant, however, because frequency-domain results are often viewed using log scales. Hence, in an experimental setting even relatively small amounts of mismatch could produce noticeable effects.

4. *CONCLUSIONS*

Direct time integration of the equations of motion along with time and frequency domain analysis of the resulting time histories has been used to study the effects of small amounts of blade-to-blade dissimilarities on the dynamics of a rotor-body system. A system of this type is governed by differential equations with periodic coefficients. This analytical approach has the advantage of giving the same sort of physical insight that one obtains from an experiment.

Small amounts of mismatch in the nonrotating, isolated blade frequencies of a rotor were found to only slightly alter the frequencies of the system. The most noticeable effect of the blade-to-blade dissimilarities was the appearence of many new peaks in the spectrum at frequencies equal to the those of the expected modes $\pm$M/rev. These side peaks are the physical manifestations of the periodic mode shapes of Floquet theory, and they illustrate what the idea of "multivalued frequencies" really means. Coupling between the previously uncoupled ζ_0 coordinate and the non-rotating coordinates comes about through these side peaks when the blades are not matched.

Because these side peaks are spaced at multiples of rotor speed from the primary modes of interest (*i.e.*, the regressing mode, the progressing mode, and collective mode) and these

modes naturally tend to be separated from each other by near multiples of 1/rev, the side peaks then appear near these modes and can potentially create frequency and damping measurement problems due to frequency contamination. This is less of a problem for soft bodies where rotor-body coupling is strong enough to move the progressing and regressing frequencies away from the uncoupled values (which have exactly 2/rev separation from each other and 1/rev separation from the collective mode). The inclusion of the rotor shaft degree of freedom greatly reduces the extent to which the rotating system modes appear in fixed system coordinates, thus easing the frequency contamination problems. This shaft freedom shifts the collective mode frequency so that even if the mode does appear in the fixed system it is less likely to interfere with any mode of interest.

REFERENCES

1. Coleman, R.P.; and Feingold, A.M.: Theory of Self-Excited Mechanical Oscillations of Helicopter Rotors With Hinged Blades. NACA Report 1351, 1958.

2. Hohenemser, K.H.; and Yin, S.K.: Some Applications of the Method of Multiblade Coordinates. *Journal of the American Helicopter Society*, vol. 17, no. 3, July 1972, pp.3-12.

3. Peters, D.A.; and Hohenemser, K.H.: Application of the Floquet Transition Matrix to Problems of Lifting Rotor Stability. *Journal of the American Helicopter Society*, vol. 16, no. 2, April 1971, pp.25-33.

4. Peters, D.A.: Flap-Lag Stability of Helicopter Rotor Blades in Forward Flight. *Journal of the American Helicopter Society*, vol. 20, no. 4, October 1975, pp.2-13.

5. Zvolanek, I.: Stability of an Unsymmetric Rotor on an Unsymmetric Support. *Journal of the American Helicopter Society*, vol. 24, no. 5, April 1979, pp.36-42.

6. Hammond, C.E.: An Application of Floquet Theory to Prediction of Mechanical Instability. *Journal of the American Helicopter Society*, vol. 19, no. 4, October 1974, pp.14-23.

7. Bousman, W.G.; and Winkler, D.J.: Application Of The Moving-Block Analysis, Paper 81-0653-CP, 22nd Structures, Structural Dynamics, & Materials Conference, Atlanta, Ga., April 1981.

8. Kane, T.R.; and Levinson, D.A.: Formulation of the Equations of Motion for Complex Spacecraft. *Journal of Guidance and Control*, vol. 3, no. 2, March-April 1980, pp.99-112.

Appendix
Equations of Motion

The equations of motion for the system shown in Figure 1 were derived by Kane's method [8] and are expressed as vector equations of the form

$$u = \dot{q}$$
$$M(u,q,t)\dot{u} = f(u,q,t)$$

where u, q, and f are column vectors, M is a symmetric matrix, and t is time. The column vector q is

$$\begin{aligned} q_i &= \zeta_i \qquad i = 1,2,\ldots,N \\ q_{N+1} &= x \\ q_{N+2} &= y \\ q_{N+3} &= s \end{aligned}$$

The elements of M are given by

$$\begin{aligned} M_{i,i} &= I_i^* + m_i l_i^{*2} \qquad i = 1,2,\ldots,N \\ M_{i,j} &= 0 \qquad i,j = 1,2,\ldots,N \qquad i \neq j \\ M_{i,N+1} &= m_i l_i^* cos(\Omega t + \psi_i + q_{N+3} + q_i) \qquad i = 1,2,\ldots,N \\ M_{i,N+2} &= m_i l_i^* sin(\Omega t + \psi_i + q_{N+3} + q_i) \qquad i = 1,2,\ldots,N \\ M_{i,N+3} &= I_i^* + m_i l_i^{*2} + m_i e_i l_i^* cos\ q_i \qquad i = 1,2,\ldots,N \\ M_{N+1,N+1} &= m_x + \sum_{i=1}^{N} m_i \\ M_{N+1,N+2} &= 0 \\ M_{N+1,N+3} &= \sum_{i=1}^{N} [m_i e_i cos(\Omega t + \psi_i + q_{N+3}) \\ &\quad + m_i l_i^* cos(\Omega t + \psi_i + q_{N+3} + q_i)] \end{aligned}$$

$$M_{N+2,N+2} = m_y + \sum_{i=1}^{N} m_i$$

$$M_{N+2,N+3} = \sum_{i=1}^{N} [m_i e_i sin(\Omega t + \psi_i + q_{N+3}) + m_i l_i^* sin(\Omega t + \psi_i + q_{N+3} + q_i)]$$

$$M_{N+3,N+3} = I_s + \sum_{i=1}^{N} (I_i^* + m_i l_i^{*2} + m_i e_i^2 + 2 m_i e_i l_i^* cos\ q_i)$$

The column vector f is given by

$$f_i = -k_i q_i - c_i u_i + T_s - m_i e_i l_i^* (\Omega + u_{N+3})^2 sin\ q_i \qquad i = 1, 2, \ldots, N$$

$$f_{N+1} = -k_x q_{N+1} - c_x u_{N+1} + F_x + \sum_{i=1}^{N} [m_i e_i (\Omega + u_{N+3})^2 sin(\Omega t + \psi_i + q_{N+3}) + m_i l_i^* (\Omega + u_{N+3} + u_i)^2 sin(\Omega t + \psi_i + q_{N+3} + q_i)]$$

$$f_{N+2} = -k_x q_{N+2} - c_x u_{N+2} + F_y - \sum_{i=1}^{N} [m_i e_i (\Omega + u_{N+3})^2 cos(\Omega t + \psi_i + q_{N+3}) + m_i l_i^* (\Omega + u_{N+3} + u_i)^2 cos(\Omega t + \psi_i + q_{N+3} + q_i)]$$

$$f_{N+3} = -k_s q_{N+3} - c_s u_{N+3} + T_s + \sum_{i=1}^{N} T_i + \sum_{i=1}^{N} [m_i e_i l_i^* (2\Omega + 2u_{N+3} + u_i) u_i sin\ q_i]$$

where F_x and F_y are applied body forces, and T_s and T_i are applied torques on the shaft and blades.

Table 1: Baseline Model Properties

Blade Properties:	$c_i = 0.0325$ N-m-sec
	$e_i = 0.0956$ m
	$I_i^* = 0.01165$ kg-m^2
	$k_i = 149.65$ N-m
	$l_i^* = 0.169$ m
	$m_i = 0.934$ kg
	$N = 3$
Soft Body Properties:	$c_x = 4.38$ N-sec/m
	$c_y = 62.75$ N-sec/m
	$k_x = 29,200.$ N/m
	$k_y = 474,600.$ N/m
	$m_x = 2.945$ kg
	$m_y = 1.706$ kg
Stiff Body Properties:	$c_x = 46.7$ N-sec/m
	$c_y = 49.6$ N-sec/m
	$k_x = 298,700.$ N/m
	$k_y = 533,550.$ N/n
	$m_x = 1.735$ kg
	$m_y = 1.646$ kg
Shaft Properties:	$c_s = 0.407$ N-m-sec
	$I_s = 0.02034$ kg-m^2
	$k_s = 338.95$ N-m

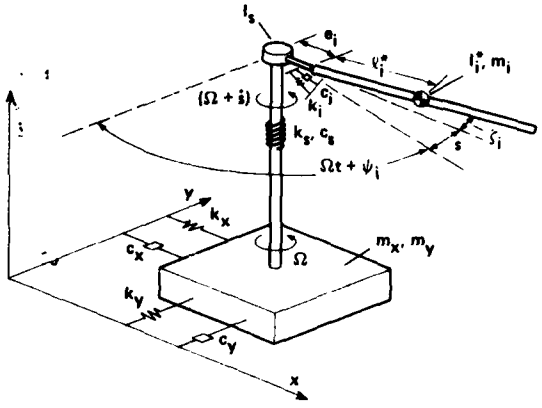

Fig. 1. System schematic.

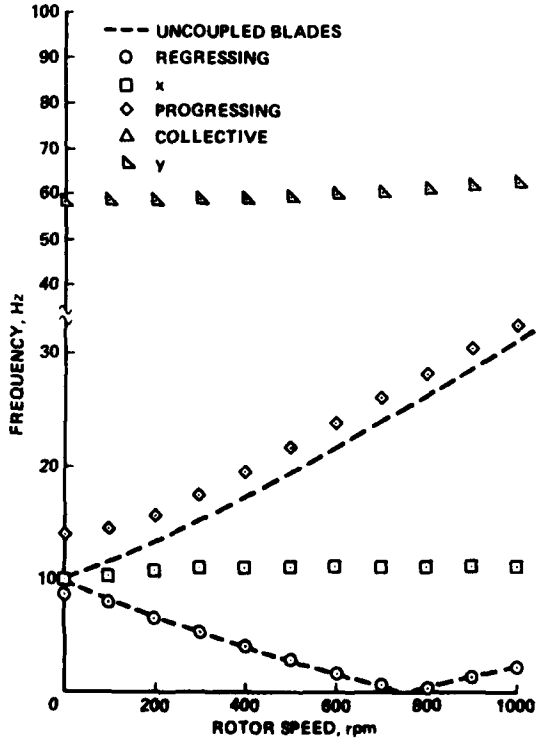

Fig. 2. Fixed system frequencies; soft body, matched blades.

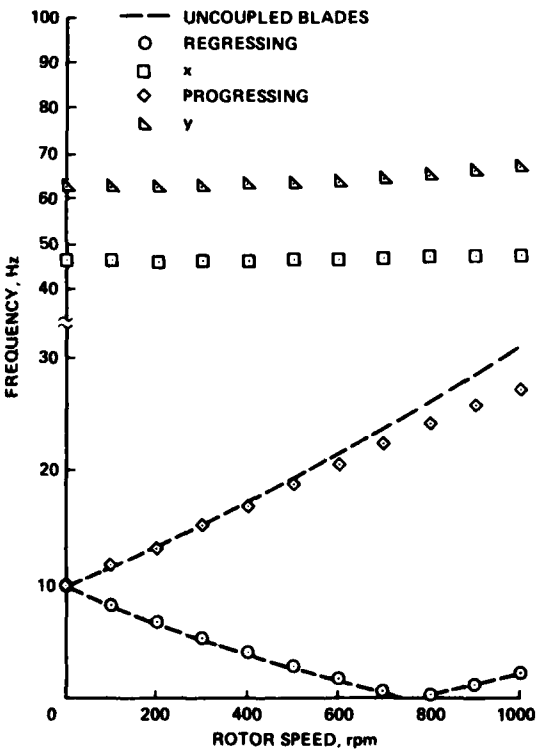

Fig. 3. Fixed system frequencies; stiff body, matched blades.

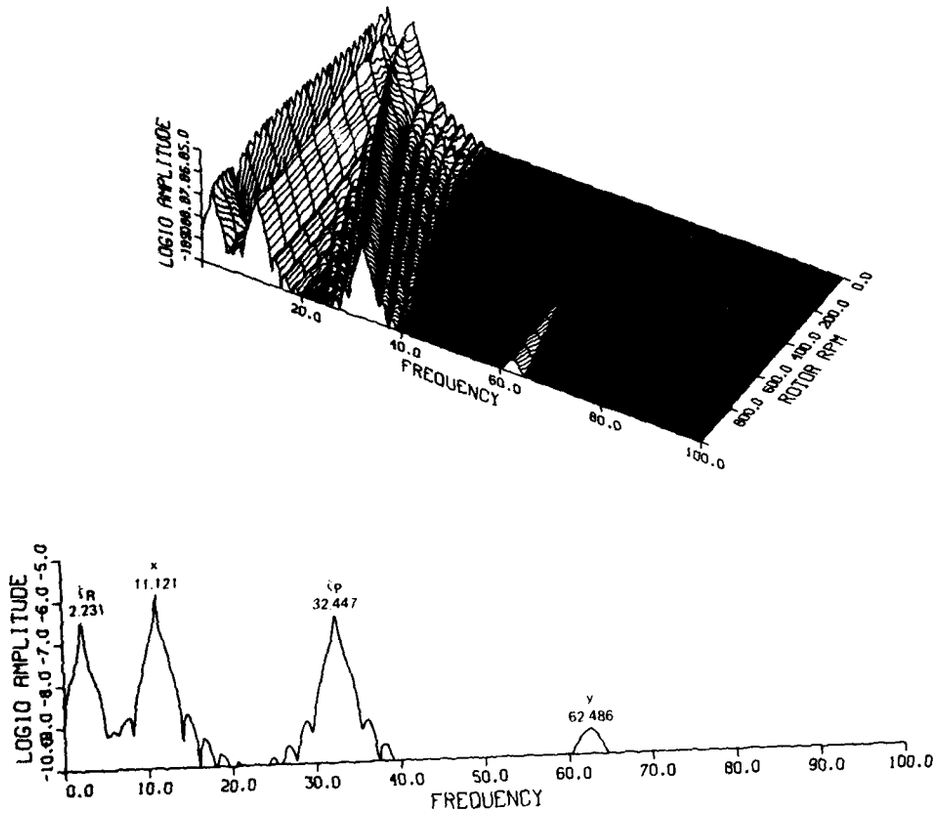

Fig. 4. Response of ζ_c coordinate to an x initial condition; soft body, matched blades. (a) As function of rpm. (b) At 1000 rpm.

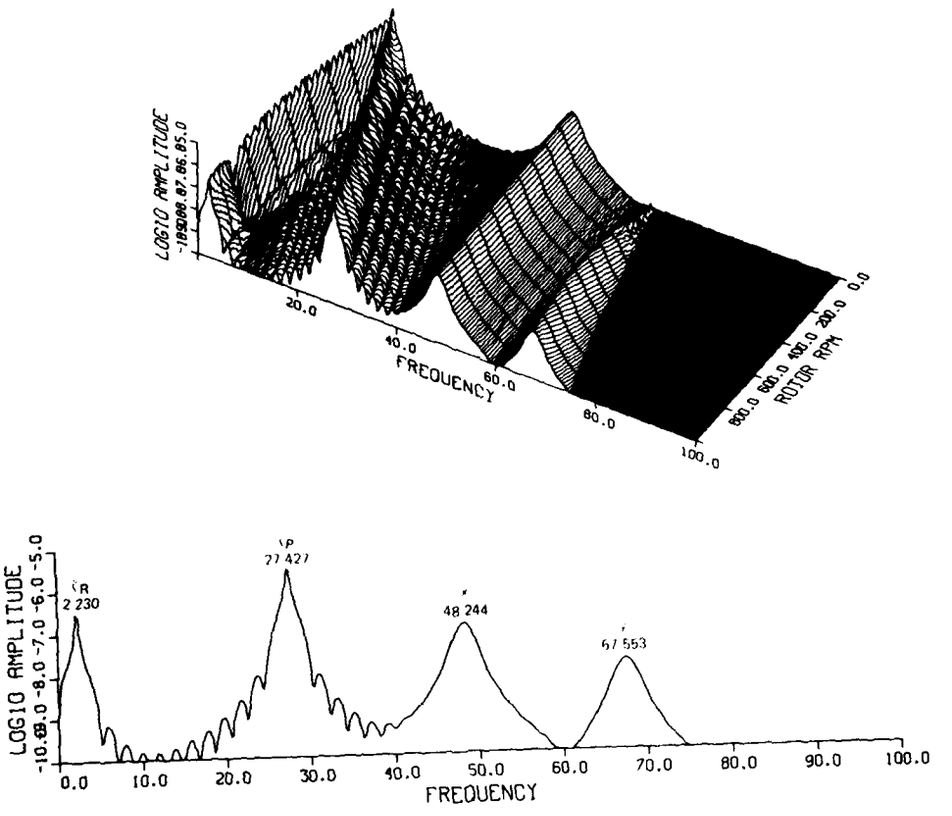

Fig. 5. Response of ζ_c coordinate to an x initial condition; stiff body, matched blades. (a) As function of rpm. (b) At 1000 rpm.

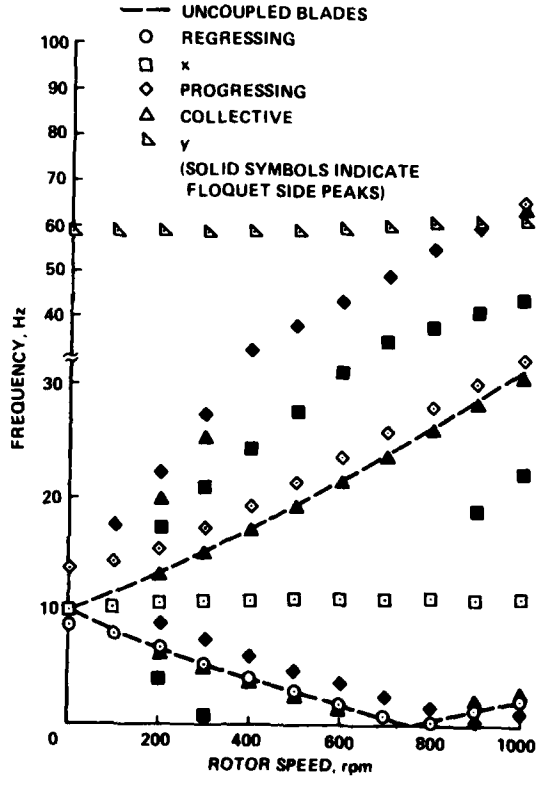

Fig. 6. Fixed system frequencies; soft body, no shaft degree of freedom, 4% mismatched blades.

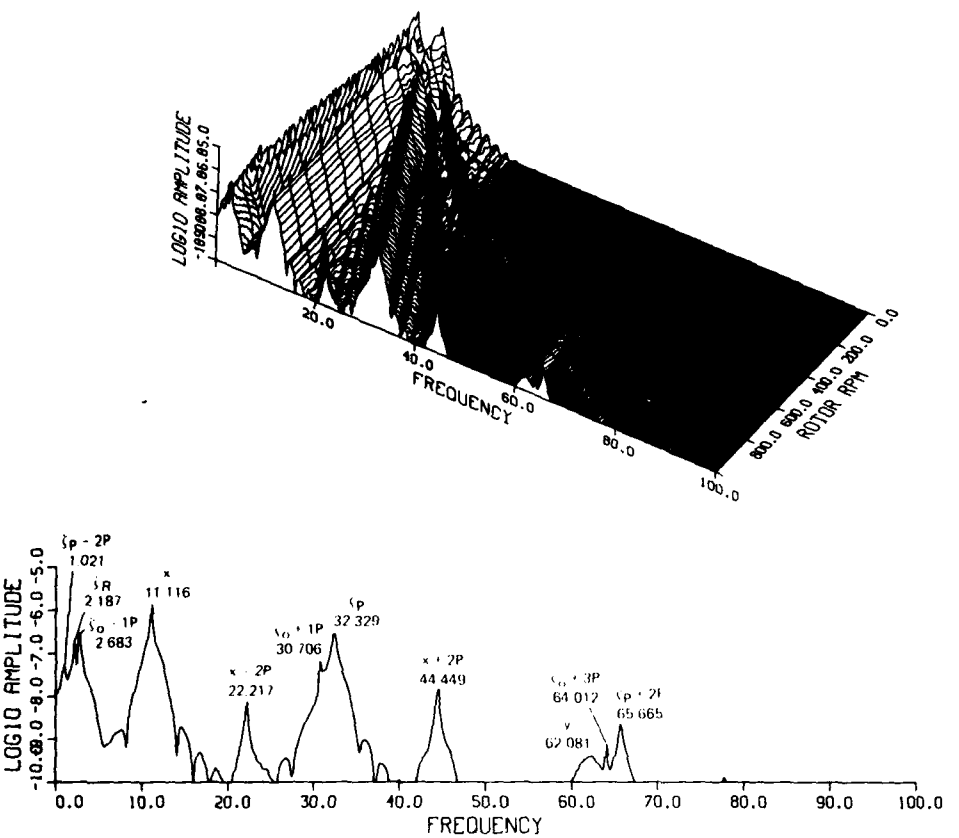

Fig. 7. Response of ζ_c coordinate to an x initial condition; soft body, no shaft degree of freedom, 4% mismatched blades. (a) As function of rpm. (b) At 1000 rpm.

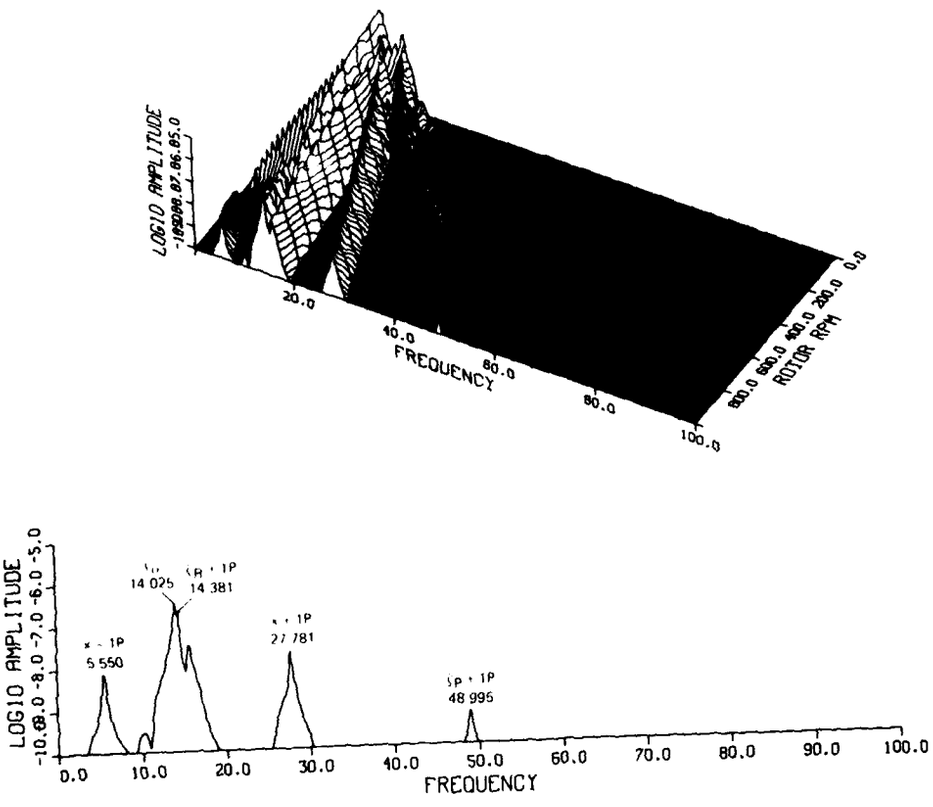

Fig. 8. Response of ζ_o coordinate to an x initial condition; soft body, no shaft degree of freedom, 4% mismatched blades. (a) As function of rpm. (b) At 1000 rpm.

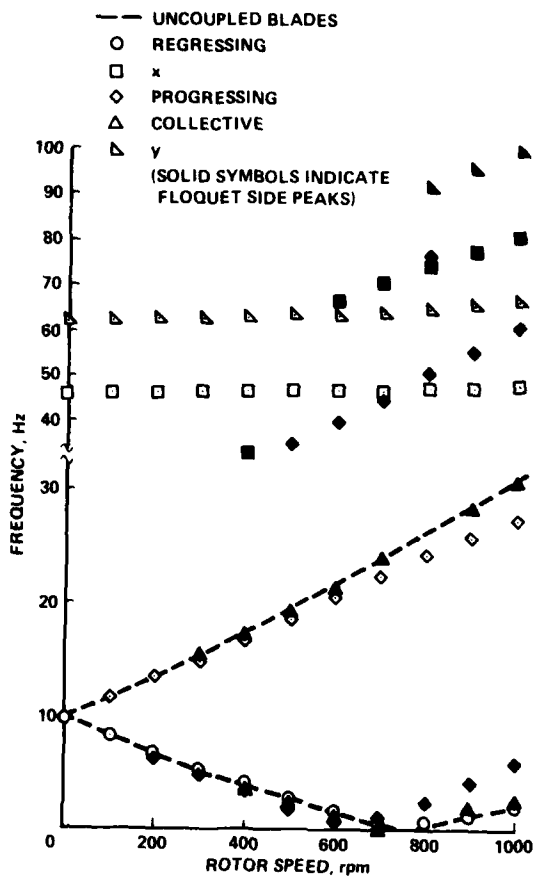

Fig. 9. Fixed system frequencies; stiff body, no shaft degree of freedom, 4% mismatched blades.

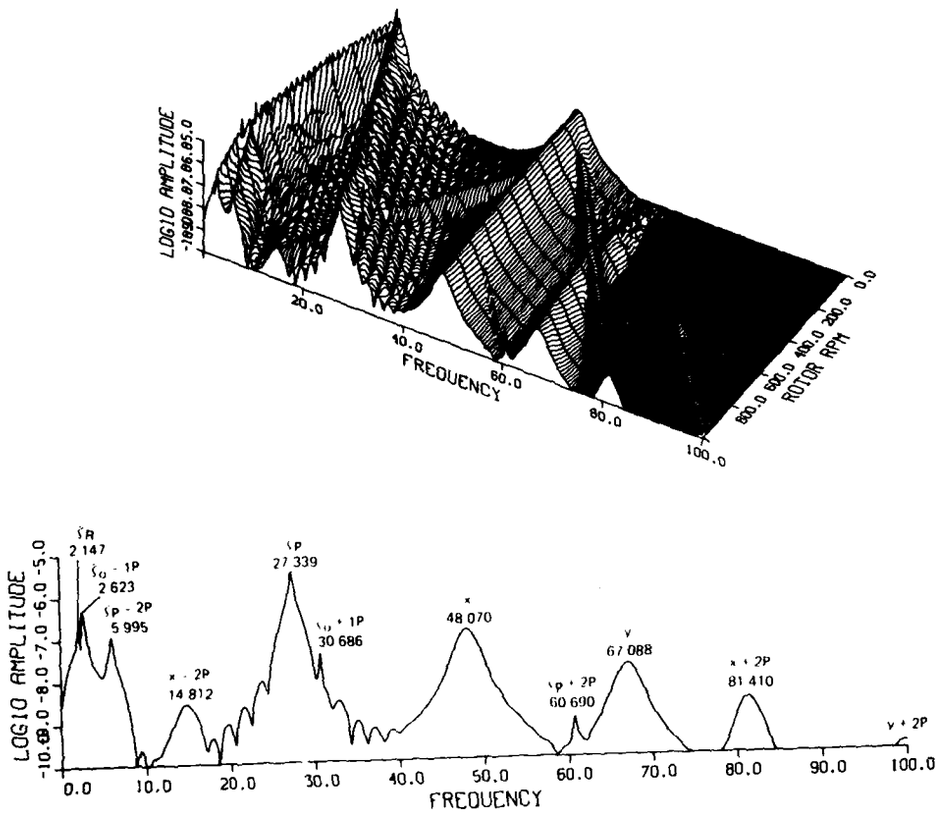

Fig. 10. Response of ζ_c coordinate to an x initial condition; stiff body, no shaft degree of freedom, 4% mismatched blades. (a) As function of rpm. (b) At 1000 rpm.

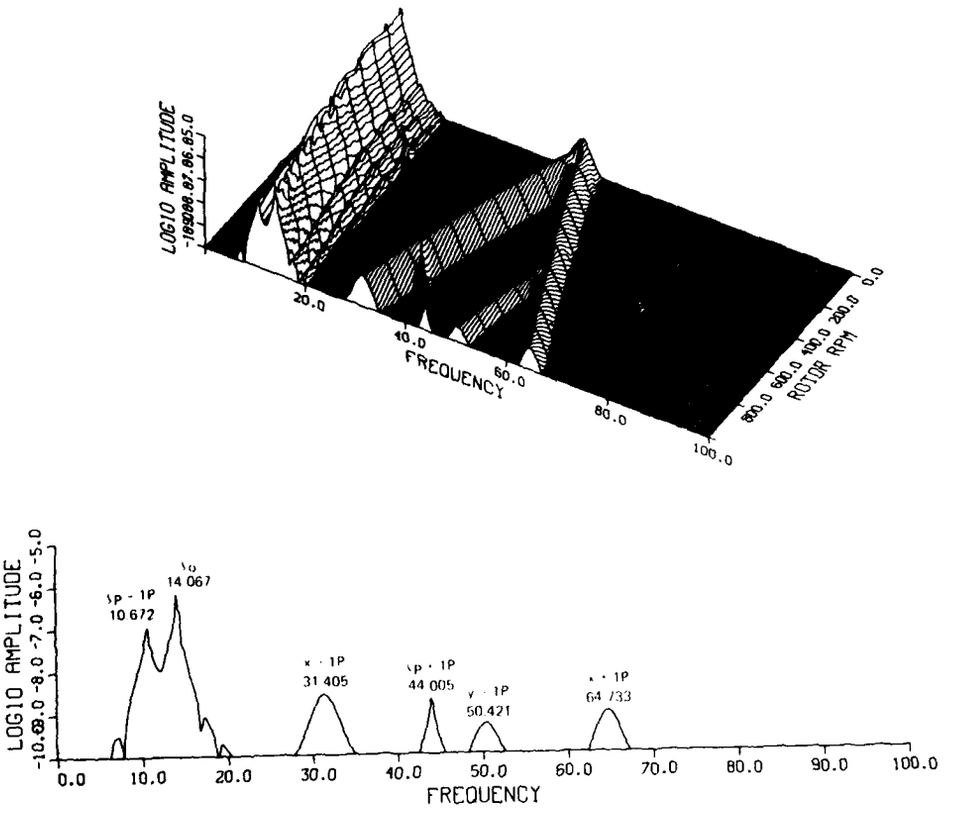

Fig. 11. Response of ζ_o coordinate to an x initial condition; stiff body, no shaft degree of freedom, 4% mismatched blades. (a) As function of rpm. (b) At 1000 rpm.

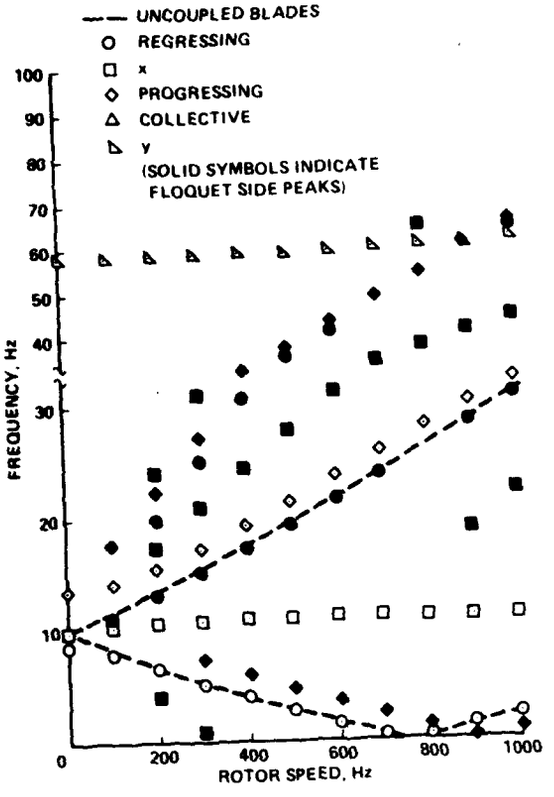

Fig. 12. Fixed system frequencies; soft body, with shaft degree of freedom, 4% mismatched blades.

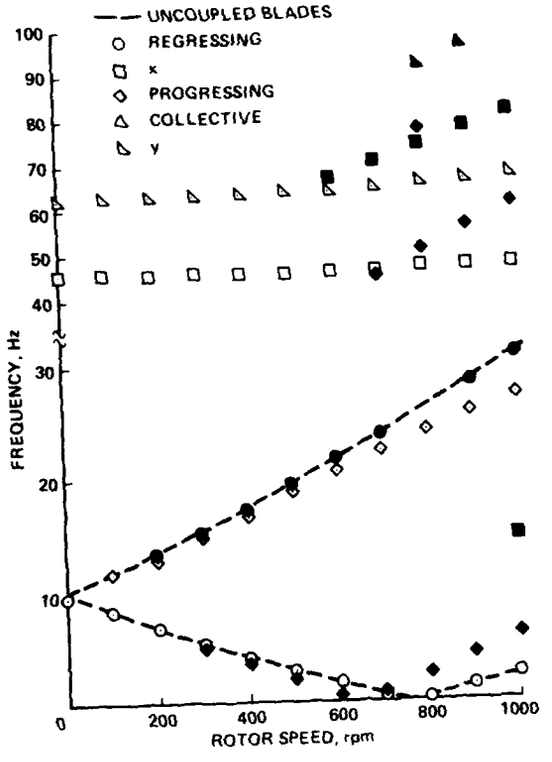

Fig. 13. Fixed system frequencies; stiff body, with shaft degree of freedom, 4% mismatched blades.

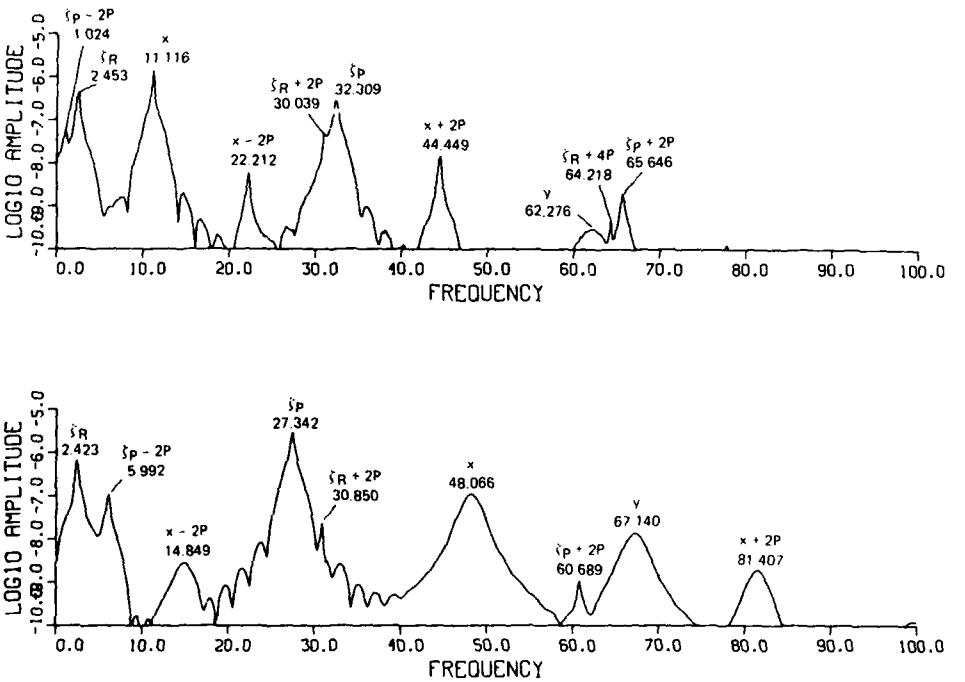

Fig. 14. Response of ζ_c coordinate to an x initial condition; at 1000 rpm, with shaft degree of freedom, 4% mismatched blades. (a) Soft body. (b) Stiff body.

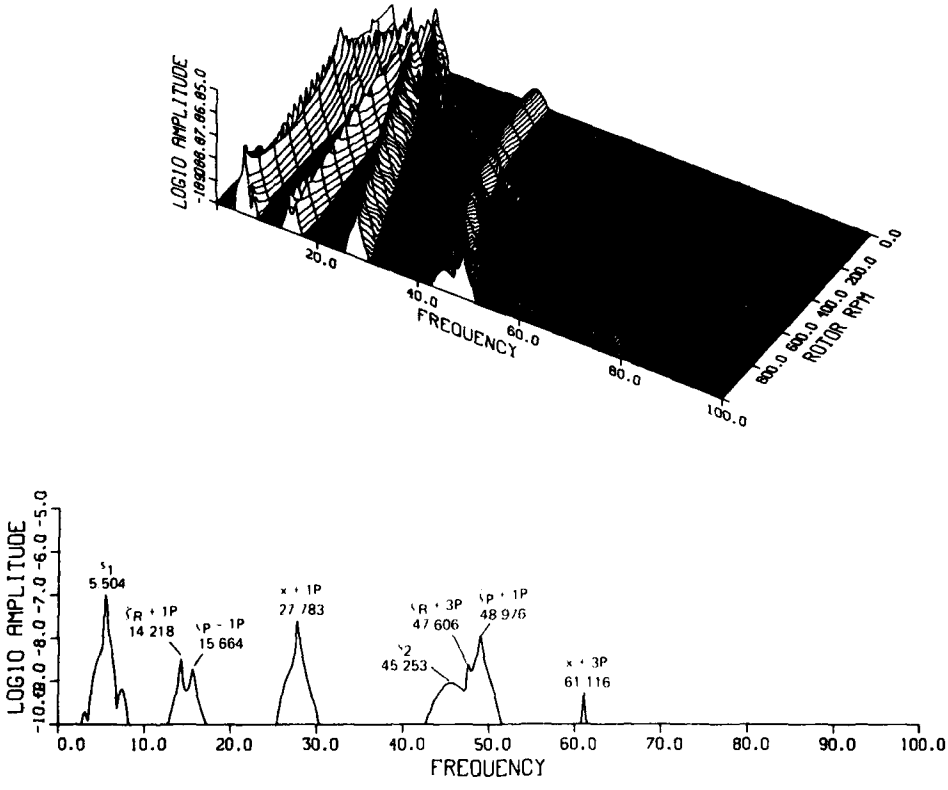

Fig. 15. Response of ζ_o coordinate to an x initial condition; soft body, with shaft degree of freedom, 4% mismatched blades. (a) As function of rpm. (b) At 1000 rpm.

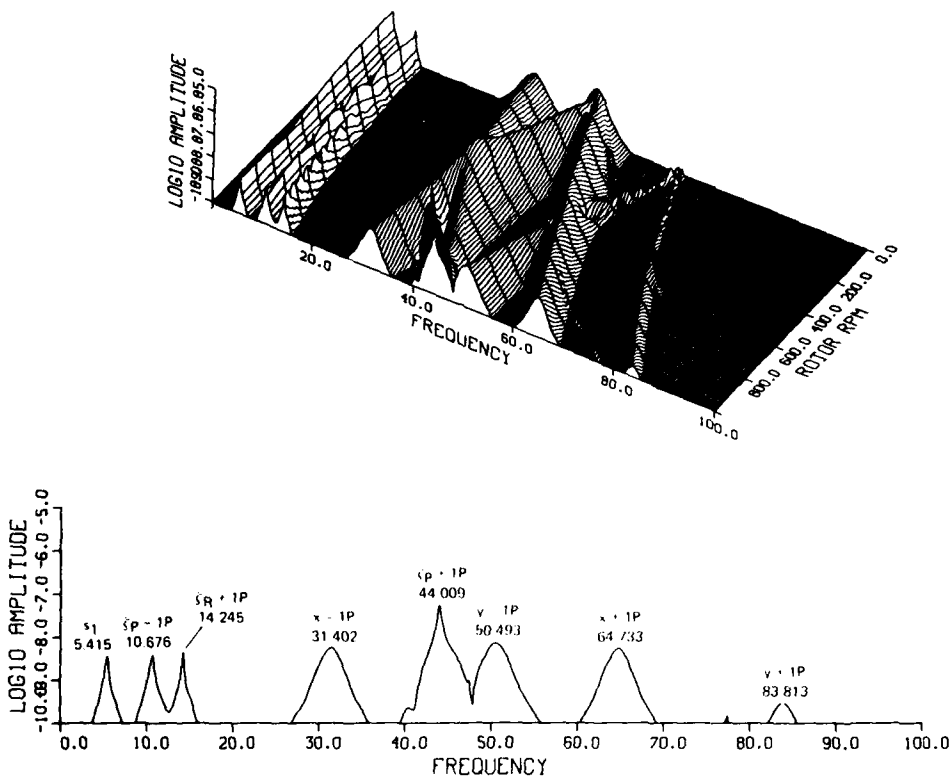

Fig. 16. Response of ζ_o coordinate to an x initial condition; stiff body, with shaft degree of freedom, 4% mismatched blades. (a) As function of rpm. (b) At 1000 rpm.

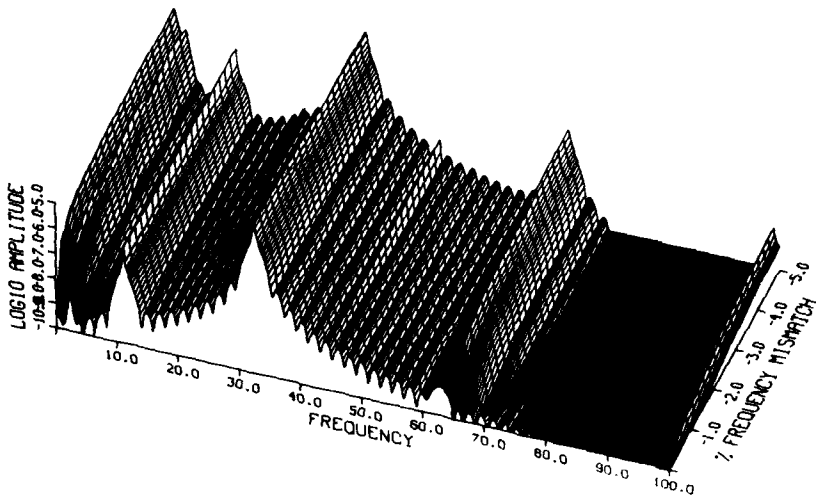

Fig. 17. Response of ζ_c coordinate to progressing excitation as a function of mismatch; soft body, no shaft degree of freedom, 1000 rpm.

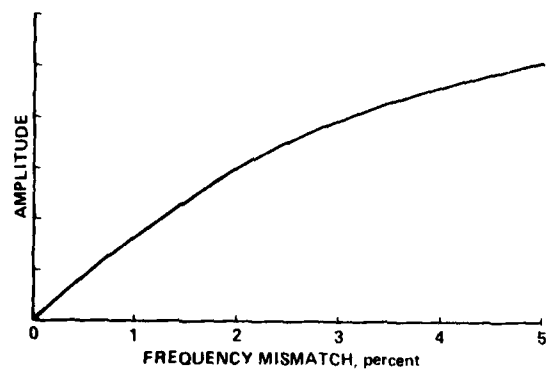

Fig. 18. Amplitude of the ζ_c coordinate progressing mode +2/rev response with as a function of mismatch, with a linear amplitude scale; soft body, no shaft degree of freedom, 1000 rpm, progressing excitation.

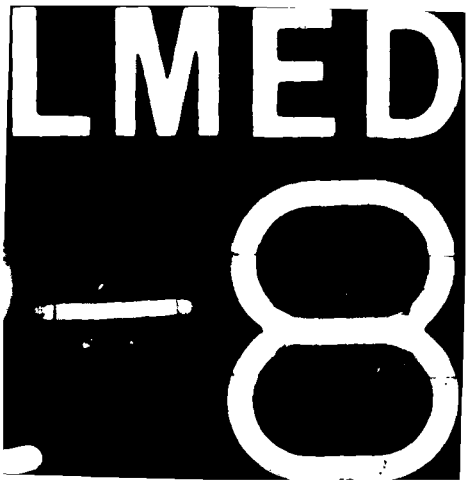
LMED
8